

# Enabling the Seamless Coordination and Synchronization of Microgrids using Batteries

Diana P. Morán-Río  
Electrical Systems Unit  
IMDEA Energy Institute  
Madrid, Spain  
diana.moran@imdea.org

Javier Roldán-Pérez  
Electrical Systems Unit  
IMDEA Energy Institute  
Madrid, Spain  
javier.rolan@imdea.org

Milan Prodanovic  
Electrical Systems Unit  
IMDEA Energy Institute  
Madrid, Spain  
milan.prodanovic@imdea.org

Aurelio García-Cerrada  
Institute for Research in Technology (IIT)  
ICAI Engineering School, Comillas Pontifical University  
Madrid, Spain  
aurelio@comillas.edu

**Abstract**—Microgrids (MGs) have become a commonly used way for renewable energy sources (RESs) integration in electrical distribution systems. These MGs are formed of a mix of RESs and batteries that can operate either in grid-forming or grid-following control modes. In these new scenarios, the transition from islanded to grid-connected mode is a challenging issue, especially if there are renewable-based grid-forming converters working at their maximum power point. In this paper, a secondary controller that enables the seamless operation of grid-forming converters with batteries is proposed. This controller allows the connection of loads and synchronisation of the MG with the main grid without the need for altering the power injected by some selected grid-forming converters (e.g., those working at their maximum power point). Meanwhile, any additional power demand is met by the batteries and shared between them according to their SoC. The main developments are tested using Simulink and simPowerSystems simulation environments.

**Keywords**—Microgrid, Synchronization, Coordination, Grid-Forming, Droop Control, Batteries.

## I. INTRODUCTION

Microgrids (MG) had been introduced to facilitate power networks reaching remote areas with high penetration of renewable resources. In these MGs, adequate stability margins, power quality indices and continuity of energy supply are key factors that should be guaranteed. In order to address all these issues, a hierarchical control scheme based on three control levels is commonly used [1]. In particular, the secondary control level coordinates the operation of all devices so that the MG can apply the high-level decisions made at the tertiary level. Among the coordination tasks, the synchronisation of the MG with the main grid is a relevant issue. Synchronisation

The work of IMDEA Energy Institute received financial support from Spanish Ministry of Science, Innovation and Universities through Juan de la Cierva Incorporación program (IJC2019-042342-I). The work has also been partially financed through the research programme S2018/EMT-4366 PROMINT-CAM of Madrid Government -Spain- with 50 % support of the European Social Fund. Diana Morán is within a PhD Collaboration agreement between Comillas Pontifical University and IMDEA Energy Institute.

becomes challenging when the MG is formed by a variety of grid-forming (GFM) and grid-following (GFL) converters, which is a common case when batteries and renewable energies coexist [2].

MG synchronization consists of making equal the phase and voltage magnitude at both sides of the point of common coupling (PCC). The most extended approach to achieve this goal is to modify the frequency and voltage commands sent by the secondary controller [3, 4]. The case where all GFM units are connected to the same bus bar or even to the PCC has been studied in detail [3]. This is a rather simple case of a power-park since the output of the secondary controller is the same as the PCC voltage, in steady state. Controllers that can synchronize devices regardless the MG topology have also been proposed in the literature [4]. In this case, a common approach is to adjust the frequency of the MG to be as close as possible to the frequency of the grid voltage. Then, when the angle difference is close to be zero, the connection is established. This strategy is not suitable for large MGs since small angle differences may cause large electrical transients. Some authors propose to change the frequency of GFM converters until the phase difference is exactly zero. Consensus algorithms represent the most common approach with this respect [4, 5]. However, this control strategy does not allow the use of power constraints and this could result in an “uneven” power sharing during the synchronisation process.

Changes in the operating point are undesirable for renewable energy sources working in their optimal power point. To avoid these changes, the power sharing between converters should be conveniently modified. Power sharing in droop dominated MGs has been widely studied in the literature [6]. The selection of the droop gains may be based on the generator ratings, economical dispatching or SoC of storage units [7]. When batteries are involved, droop gains are commonly chosen to be inversely proportional to the SoC [7]. The commands sent by the secondary controller in order to synchronize the MG alter the operating point of GFM units during islanding

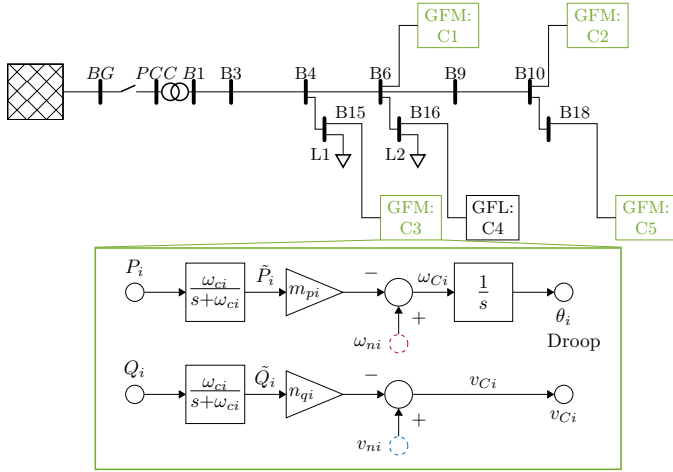


Fig. 1. Single line diagram of the MG studied in this work, including the primary controller of GFM devices.

operation [8]. In this case, batteries are an adequate option to smooth the transition between operating modes [9]. Therefore, batteries can be used to absorb/inject the necessary energy while the rest of GFM units maintain their operating points. Nevertheless, this aspect has not been studied in detail in the literature [10].

In this paper, a secondary controller for battery and distributed energy resource (DER) coordination in MGs is presented. The proposed secondary controller maintains the operating point of some selected GFM devices constant during the synchronization process and, also, when load and generation are modified. The energy needed to achieve these changes is supplied from batteries interfaced by droop-controlled converters according to their SoC. To avoid undesired changes in the operating point, additional changes to the droop characteristic are proposed. The developments are validated by using Simulink and simPowerSystems.

## II. OVERVIEW

### A. Application Description

Fig. 1 shows a diagram of the MG studied in this paper while Fig. 2 shows the secondary controller. This case represents a simplified version of a Cigré low-voltage distribution benchmark for the integration of DERs [11]. The MG is connected to the main grid at the PCC, which is located in node  $B0$ . The system consists of a feeder and a transformer that feeds two loads ( $L1$  and  $L2$ ). In this MG, several DERs and batteries are connected. Batteries are connected by using GFM converters ( $C2$ ,  $C3$  and  $C5$ ), while DERs are connected by using either GFM or GFL converters ( $C1$  is GFM and  $C4$  is GFL). All the converters have an  $LCL$  filter.

### B. Control Overview

GFL converters are controlled by means of PI controllers that regulate the current through the inner inductance of the  $LCL$  filter. The converter is synchronized to the MG voltage by using of a phase-locked loop (PLL).

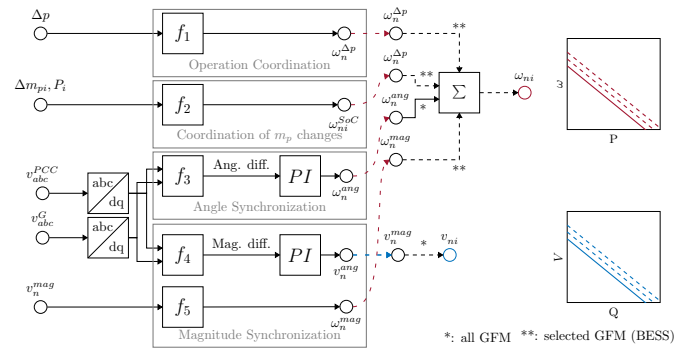


Fig. 2. Secondary controller. Generation of voltage and frequency set-points and adjustment of droop curves.

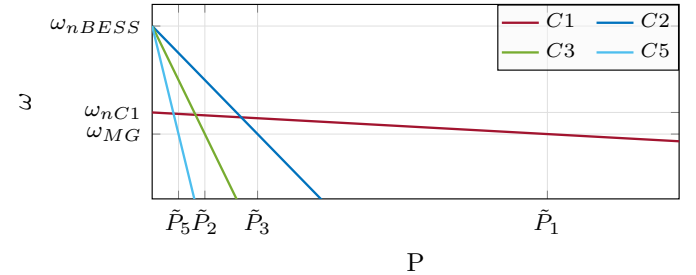


Fig. 3. Example of droop curves for a MG with different GFM units.  $\omega_{MG}$  is the MG frequency in steady state.

GFM converters have a current loop that regulates the current through the inner inductance of the  $LCL$  filter and a voltage loop that regulates the voltage across the filter capacitor. Quasi-stationary virtual impedances are used to facilitate their paralleled operation [12]. Also, GFM converters include conventional  $P - f$  and  $Q - V$  droop controllers:

$$\omega = \omega_n - m_p \tilde{P}, \quad V = V_n - n_q \tilde{Q}, \quad (1)$$

where  $\omega_n$  and  $V_n$  are the no-load frequency and voltage magnitude, and  $m_p$  and  $n_q$  are the droop characteristics. The equivalent block diagram is depicted in Fig. 1. In that diagram,  $\tilde{P}$  and  $\tilde{Q}$  are the filtered values of the active and reactive powers injected by the unit:

$$\tilde{P} = \frac{1}{s/\omega_c + 1} P, \quad \tilde{Q} = \frac{1}{s/\omega_c + 1} Q, \quad (2)$$

where  $\omega_c$  is the cut-off frequency of the filter. Power sharing among GFM units is performed according to the droop coefficients ( $m_{pi}$ , where  $i$  refers to the specific unit). An example of power-frequency characteristics is presented in Fig. 3. The values of  $m_{pi}$  and  $\omega_{ni}$  define the power flow among GFM units and the MG frequency  $\omega_{MG}$ .

### C. Battery Modelling and Control

The converters  $C2$ ,  $C3$  and  $C5$  have batteries in their dc sides. Batteries are represented as constant voltage sources with a voltage level equal to the open circuit voltage of the battery. This assumption is commonly accepted for lithium-ion batteries when the SoC is between 20% and 80% [13]. The

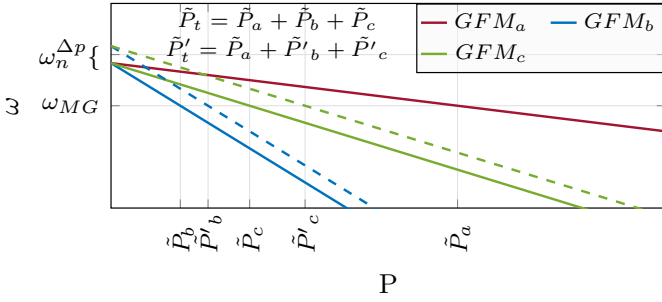


Fig. 4. Adjustment of droop curves for power sharing between the units and for maintaining the same MG frequency. Only three GFM are considered here.

SoC of the batteries is estimated by using the basic Coulomb counting method [14, 15]:

$$SoC_i = SoC_{0i} - \frac{1}{C_i} \int i_{DCi} dt, \quad (3)$$

where  $SoC_i$  is the SoC of the battery,  $SoC_{0i}$  is its initial value,  $C_i$  is the capacity of the battery and  $i_{DCi}$  is the output current of the battery.

Batteries are operated as GFM converters. The droop coefficients ( $m_{pi}$ ) are updated according to the SOC of each unit [14, 16]:

$$m_{pi} = \frac{m_{p0}}{SoC_i^n}, \quad \text{if } P_i \geq 0, \quad (4)$$

$$m_{pi} = m_{p0} SoC_i^n, \quad \text{if } P_i < 0, \quad (5)$$

where  $m_{p0}$  is the initial value of  $m_p$ .

#### D. Methodology Overview

Traditionally, the secondary control is performed by adjusting just the values of  $\omega_{ni}$  and  $V_{ni}$  (see Fig. 2) [17]. Then, the additional power required during transients it is taken from all the GFM units and this may take some of these GFM units out of their maximum power point. Contrary, the proposed secondary controller maintains the initial power-sharing ratios and distributes the additional active power among the batteries, according to their SoC. To achieve these power sharing objectives,  $\omega_{ni}$  and  $V_{ni}$  are modified by the secondary controller. As  $m_{pi}$  is updated according to the SoC of the batteries, there would be changes in the operating point of the MG if no countermeasures are taken. The solution explored in this work is to recalculate  $\omega_{ni}$  and  $V_{ni}$  to take this effect into consideration.

### III. PROPOSED CONTROL

In this section, the control algorithm presented in Fig. 2 is explained. First, the coordination of devices in the presence of load variations is explained. Then, the method to adapt the value of  $m_{pi}$  according to the SoC without modifying the operating point is depicted. Angle synchronisation is explained subsequently. Finally, voltage equalisation is presented.

#### A. Coordination of Batteries for Power Sharing

In order to share load variations among several batteries the value of  $\omega_{ni}$  in each of these batteries should be adjusted.

The initial total power delivered by the GFM converters ( $\tilde{P}_t$ ) results in a determined MG frequency ( $\omega_{MG}$ ). However, when the power demand changes, the batteries ( $GFM_b$ ,  $GFM_c$  and  $GFM_d$ ) have to shift up or down their droop curves to compensate the power variation. For simplicity, only the demand increase case is considered here. The droop curves describing this situation are depicted in Fig. 4. The shift in  $\omega_{ni}$  ( $\omega_n^{\Delta p}$ ) is the value needed to compensate the frequency droop that correspond to a power variation of  $\Delta p = \tilde{P}'_t - \tilde{P}_t$ . Here,  $\omega_n^{\Delta p}$  is calculated as the frequency droop that would appear if a single device with a similar droop injected  $\Delta p$ .

The equivalent droop obtained when more than one GFM is connected to MG can be calculated as follows [18]:

$$\frac{1}{m_p^{eq}} = \sum_i \frac{1}{m_{pi}}.$$

As a consequence,  $\omega_n^{\Delta p}$  is calculated as:

$$\omega_n^{\Delta p} = f_1(\Delta p) = \frac{1}{\sum_i \frac{1}{m_{pi}}} \Delta p. \quad (6)$$

When this criteria is applied, the batteries absorb power variations without altering the operating point of the remaining GFM units. This strategy can be applied when changes in load or generation are scheduled, or when the MG is being synchronized. If a controllable load is connected/disconnected,  $\omega_n^{\Delta p}$  is applied simultaneously to all the battery units. Similarly, when the MG consumption is constant, but the generation varies according to a certain command, that command can be used to calculate  $\Delta p$  and  $\omega_n^{\Delta p}$ , instantaneously. This strategy will be applied in the following sections to keep the same operating point while the MG is being synchronized.

#### B. Adjustment of $m_{pi}$ According to the SoC

When the droop gains are modified the equilibrium point of the MG will change as well. In this case, it is necessary to change both  $m_{pi}$  and  $\omega_{ni}$  to maintain the frequency and the power equilibrium. For each battery, the frequency before the change in  $m_{pi}$  can be calculated as in (7). After updating the value of  $m_{pi}$  with  $m'_{pi}$ , the frequency is calculated as in (8), which includes the additional term  $\omega_n^{SoC}$ . By manipulating (7) and (8), the expression for  $\omega_n^{SoC}$  is obtained, in (10).

$$\omega_i = \omega_{ni} - m_{pi} P_i, \quad (7)$$

$$\omega_i = \omega_{ni} - m'_{pi} P_i + \omega_n^{SoC}, \quad (8)$$

$$m_{pi} P_i = m'_{pi} P_i + \omega_n^{SoC}, \quad (9)$$

$$\omega_n^{SoC} = f_2(\Delta m_{pi}, P_i) = P_i (m'_{pi} - m_{pi}). \quad (10)$$

The use of these expressions ensures that the load variation is shared among the batteries according to the new droop values.

#### C. PCC Voltage Phase Synchronisation

Phase synchronization is achieved when the phases of the PCC voltage and the grid are the same, in steady state. In this case, the MG and the grid frequency will also be the same. Phase synchronization is carried out by accelerating or decelerating the frequency of GFM converters.

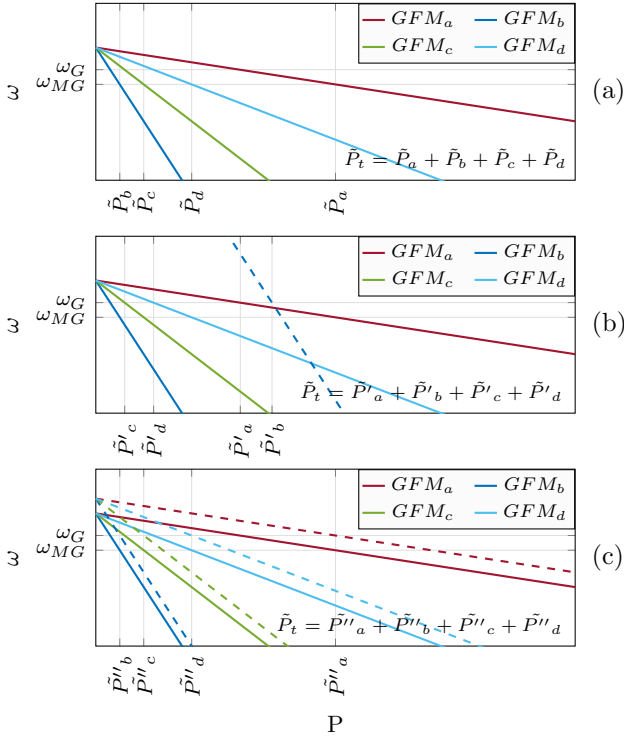


Fig. 5. MG frequency adjustment by modifying  $\omega_{ni}$ . (a) At operating point GFM units deliver  $\tilde{P}_t$  and the MG frequency is  $\omega_{MG}$ . Frequency settles at  $\omega_G$  by changing the droops of (b) only one device ( $GFM_b$ ) and (c) all the devices.

Fig. 5 (b) and (c) show two different ways to adjust  $\omega_{ni}$  to make  $\omega_{MG}$  equal to  $\omega_G$ . In Fig. 5 (b), only  $\omega_{ni}$  of one device is modified. After the change in  $\omega_{ni}$ , the GFM devices inject the same total amount of power as before the synchronisation ( $\tilde{P}_t$ ) and the MG frequency has increased up to  $\omega_G$ . Since only the frequency of one device was modified, the power sharing among the GFM units change. In contrast, Fig. 5 (c) shows the droop curves when all the GFM units are adjusted so that the power sharing among units is kept constant. In this case, the MG frequency is also  $\omega_G$ . However, there are no modifications in the power sharing compared to the original scenario (Fig. 5 (a)).

The values of  $\omega_{ni}$  are sent via communications from the secondary controller. For that purpose, a PI was applied over the angle difference between the PCC and the grid voltage, as shown in Fig. 2. The angles can be calculated as follows:

$$\theta_G = \arctan \frac{v_q^G}{v_d^G}, \quad \theta_{PCC} = \arctan \frac{v_q^{PCC}}{v_d^{PCC}}. \quad (11)$$

The angle difference is defined as:

$$\delta = f_3(v_{dq}^G, v_{dq}^{PCC}) = \theta_G - \theta_{PCC}. \quad (12)$$

Park transformations are done by using the angle of one of the reference frames. This angle can be chosen arbitrarily since the angle difference between the voltage space vectors does not depend on the reference frame selected.

The approach presented here for synchronizing the MG with the grid does not change the operating point significantly. However, slight changes may appear as some loads

may change their consumption according to the frequency. However, these changes are usually small.

#### D. PCC Voltage Equalisation

In order to synchronize the voltage magnitude of the MG and the grid while keeping constant the voltage profile, all the values of  $v_{ni}$  should be modified. First, the voltage magnitude difference is calculated as:

$$\Delta U = f_4(v_{dq}^G, v_{dq}^{PCC}) = U^G - U^{PCC}, \quad (13)$$

where

$$U^G = \sqrt{v_d^{G^2} + v_q^{G^2}}, \quad U^{PCC} = \sqrt{v_d^{PCC^2} + v_q^{PCC^2}}. \quad (14)$$

A PI controller is applied at the secondary level over  $\Delta U$ . The output of this PI controller is the voltage setting of the GFM converters ( $v_{ni}$ ). There might be more advanced criteria to change the setting points for the droops such as improving the reactive power sharing during the transient. This is not studied here, but it is of interest for future research.

The change in MG voltage varies the power that the loads absorb. If this is not compensated, the load will be shared among all GFM units according to their droop constants. To guarantee that all the batteries inject or absorb that specific value of the power, it should be taken into consideration for calculating  $\omega_{ni}$ . This is addressed in the following section.

1) *Estimation of Power Variation:* The variation in the power consumed by the MG is mainly caused by the variation in the MG voltage. In order to calculate and compensate that term, an expression that links the voltage variation with the power consumption is derived here. For that purpose, it is assumed that the voltage magnitude and its variation is equal in all the nodes. Under this consideration, a linearised expression that links the power absorbed by the loads and the MG voltage can be obtained:

$$p_i = \frac{v_i^2}{r_i}, \quad \Delta p_i \approx \frac{dp_i}{dv_i} \Delta v_i. \quad (15)$$

By manipulating (15), then

$$\Delta p_i = \frac{2v_{io}}{r_{io}} \Delta v_i, \quad \text{and} \quad \Delta p_i = \frac{2p_{io}}{v_{io}} \Delta v_i, \quad (16)$$

where subscript  $o$  refers to ‘‘operating point’’. The total power variation of the MG is then the total additional power consumed by the loads:

$$\Delta p = \sum_i \Delta p_i = \sum_i \left( \frac{2p_{io}}{v_{io}} \Delta v_i \right). \quad (17)$$

Finally, (17) can be simplified as follows:

$$\Delta p \approx \frac{2 \sum_i p_{io}}{v_o^{PCC}} \Delta v^{PCC}. \quad (18)$$

Since the internal voltage controllers of the converters are much faster than secondary controller, it is assumed that  $v_{ni}$  is applied directly to the MG. Then:

$$\Delta p \approx \frac{2 \sum_i p_{io}}{v_o^{PCC}} v_n^{mag}. \quad (19)$$

The power estimation presented in (19) is combined with the expression in (6) in order to update the battery droops. Then, the extra power need would be compensated:

$$\omega_n^{mag} = f_5(v_n^{mag}) = \frac{1}{\sum_i \frac{1}{m_{pi}}} \frac{2 \sum_i p_{io}}{v_o^{PCC}} v_n^{mag}. \quad (20)$$

### E. Controller Implementation

The implementation diagram of the proposed controller is presented in Fig. 2. PI controllers are used during synchronization to reduce magnitude and phase differences. In the coordination process, droop parameters are calculated according to (23) and (10). The voltage droop is adjusted in all GFM devices by using the following expression:

$$v_n^{BESSi} = v_n^{geni} = v_n^{mag}. \quad (21)$$

However, for the case of the frequency,  $\omega_{ni}$  takes different values depending on the type of GFM device. In generator units,  $\omega_{ni}$  only depends on the angle synchronization loop. Meanwhile, in battery units  $\omega_{ni}$  depends on the coordination controller, the controller that updates  $m_{pi}$  according to SoC, the angle and voltage synchronization loops:

$$\omega_n^{geni} = \omega_n^{ang}, \quad (22)$$

$$\omega_n^{BESSi} = \omega_n^{\Delta p} + \omega_{nSoC} + \omega_n^{ang} + \omega_n^{mag}. \quad (23)$$

### F. Adjusting the Synchronisation Speed

Synchronization speed can be modified by adjusting the proportional and integral gains of the corresponding PI controllers. For synchronising the angle, the  $PI - f$  controller can be designed to have similar bandwidth to that of the primary controllers since they are decoupled. In contrast, fast voltage controllers result in low accuracy of power estimations. Therefore, it is recommended to limit their speed. Additional studies should be carried out to address this aspect in more detail.

## IV. CONTROLLER VALIDATION

### A. Case Study

The proposed controller was applied to the MG presented in Fig. 1. The controller was implemented in a simulator that was developed in Matlab/Simulink and simPowerSystems. It included averaged models of the converters and several implementation details. The MG data can be found in [11].

### B. MG Coordination

Fig. 6 shows transient response of the active and reactive powers injected by each device for different conditions. Fig. 6 (a) and (b) present the transients of the power when a change in the load of 3 kW is applied at  $t = 5$  s and the proposed controller is applied. It can be seen that the inertial response of the converters does not change. This means that all the GFM converters are injecting power at the same time. However, after few seconds the batteries (C2, C3 and C5) inject all the power demanded by the load while C1 (GFM) returns to its original operating point. The generation change is modelled as a ramp in Fig. 6 (c) and (d). In this

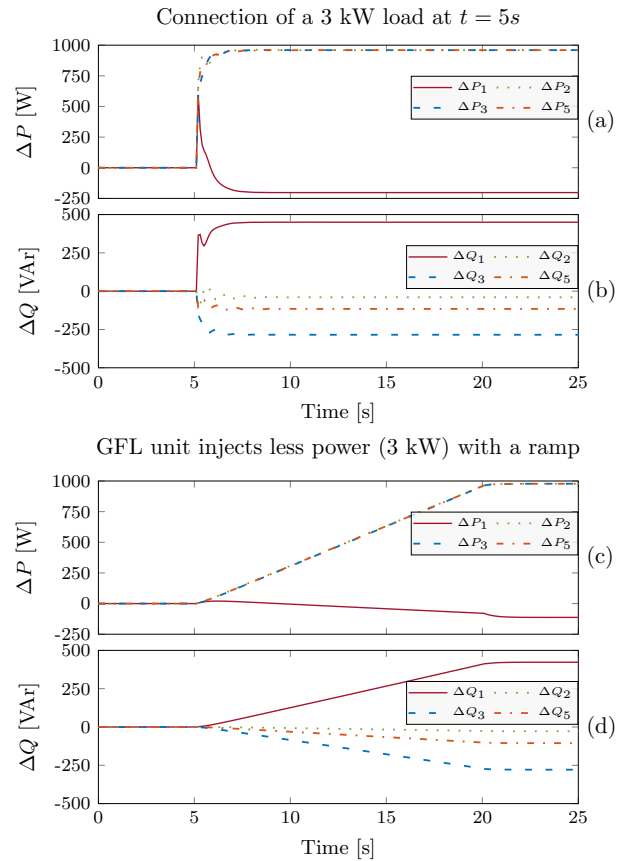


Fig. 6. (a) Active and (b) reactive power variations when a 3 kW load is connected. (c) Active and (d) reactive power variations when a GFL unit decreases 3 kW its power output, following a ramp.

case, the command sent to the GFL unit is used by the secondary controller to adapt the battery droops. In this way, batteries inject the additional energy needed by the MG and the remaining GFM units retain their operating point. Since the change in the generation conditions is gradual, the inertial response of the GFM negligible.

### C. Microgrid Synchronization

Fig. 7 shows the synchronization process of the PCC voltage (both magnitude and angle) with the grid voltage. It can be seen that both the magnitude and angle are synchronized simultaneously (Fig. 7 (a) and (b)). PI controllers have been designed to achieve the synchronisation in less than ten seconds. Additionally, the resistive part of the virtual impedance has been reduced to the lowest possible value that enables a stable operation of the MG. This allows to limit the power injected/absorbed by GFM 1 during the synchronization process. Fig. 7 (c) shows that the power estimation method only accounts for the steady state power variation. Therefore, as the speed of the synchronization process increases, some dynamics are not captured by the estimation and GFM units may exchange some additional (undesired) power with the MG.

When the PCC and the grid voltage are synchronized (at  $t = 7$  s, approximately) the MG is connected to the grid by closing the main switch. Fig. 7 (d) shows the transient of the

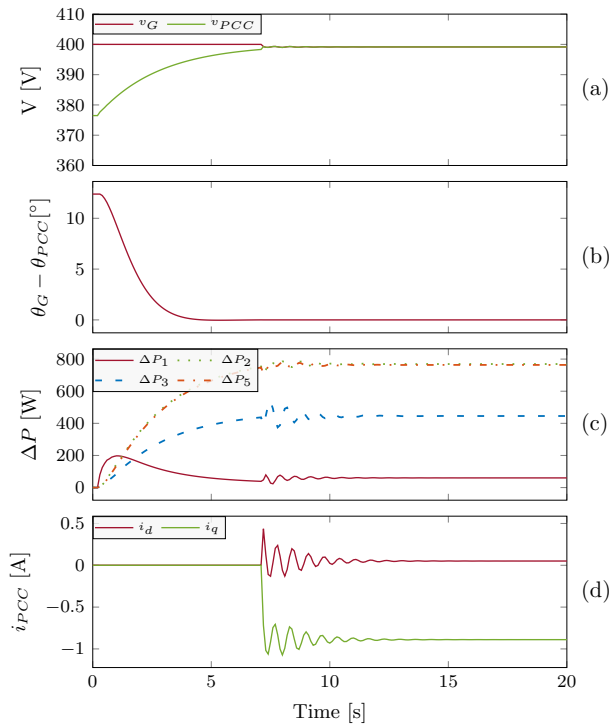


Fig. 7. Synchronization of the PCC voltage and the grid voltage. (a) Voltage magnitude, (b) angle difference, (c) power variation of GFM converters and (d) current exchanged with the grid.

current through the line that interconnects the MG with the grid. The exchange of energy at the connection point and the transient response depend on both the strength of the main grid and the primary controllers. However, as the MG is well synchronized, the power exchange is almost negligible.

## V. CONCLUSION

In this paper, a controller that enables seamless operation of GFM units in a MG during transitions and transients has been presented. Both synchronization to an external grid and coordination during the connection/disconnection of loads and generation have been addressed. It has been explained how the proposed controller modifies the set points of the GFM units to achieve its objectives. In the presented scenarios, the objective of the controller is to coordinate the GFM units so that the batteries absorb/inject the necessary energy while other GFM units keep their operating points constant.

Theoretical and simulation results have shown the controller successfully maintained the active power operating points of the selected GFM converters during load variations and when the MG was synchronized with the main grid. Only small deviations of the active power were observed, that occurred because of the system losses. Reactive power sharing has not been addressed in this work. However, optimization of the reactive power flow during the aforementioned conditions might be of interest for further research. It is worth noting that reactive power sharing is a more complex issue, especially when Q-V droops are used because the voltage is not a global variable as it is the frequency.

## VI. APPENDIX

The corresponding data files are available at [19].

## REFERENCES

- [1] N. Hatziargyriou, *Microgrids: architectures and control*. John Wiley & Sons, 2014.
- [2] C. Cho, J.-H. Jeon, J.-Y. Kim, S. Kwon, K. Park, and S. Kim, "Active synchronizing control of a microgrid," *IEEE Transactions on Power Electronics*, vol. 26, no. 12, pp. 3707–3719, 2011.
- [3] A. Micallef, M. Apap, C. Spiteri-Staines, and J. M. Guerrero, "Single-phase microgrid with seamless transition capabilities between modes of operation," *IEEE Trans. on Sm. Grid*, vol. 6, no. 6, pp. 2736–2745, 2015.
- [4] D. Shi, X. Chen, Z. Wang, X. Zhang, Z. Yu, X. Wang, and D. Bian, "A distributed cooperative control framework for synchronized reconnection of a multi-bus microgrid," *IEEE Transactions on Smart Grid*, vol. 9, no. 6, pp. 6646–6655, 2018.
- [5] Y. Du, H. Tu, and S. Lukic, "Distributed control strategy to achieve synchronized operation of an islanded mg," *IEEE Transactions on Smart Grid*, vol. 10, no. 4, pp. 4487–4496, 2019.
- [6] S.-J. Ahn, J.-W. Park, I.-Y. Chung, S.-I. Moon, S.-H. Kang, and S.-R. Nam, "Power-sharing method of multiple distributed generators considering control modes and configurations of a microgrid," *IEEE Transactions on Power Delivery*, vol. 25, no. 3, pp. 2007–2016, 2010.
- [7] J. M. Guerrero, J. C. Vasquez, J. Matas, M. Castilla, and L. Garcia de Vicuna, "Control strategy for flexible microgrid based on parallel line-interactive ups systems," *IEEE Transactions on Industrial Electronics*, vol. 56, no. 3, pp. 726–736, 2009.
- [8] J. He, Y. W. Li, J. M. Guerrero, F. Blaabjerg, and J. C. Vasquez, "An islanding microgrid power sharing approach using enhanced virtual impedance control scheme," *IEEE Transactions on Power Electronics*, vol. 28, no. 11, pp. 5272–5282, 2013.
- [9] A. Sunjaq, P. Chen, M. Bongiorno, R. Majumder, and J. Svensson, "Frequency Control by BESS for Smooth Island Transition of Hydro-Powered Microgrid," 4 2022.
- [10] J.-Y. Choi and D. Won, "Advanced active power control considering the characteristics of distributed energy resources in microgrid," *Journal of Electrical Engineering & Technology*, vol. 11, pp. 1100–1107, 2016.
- [11] K. Strunz, E. Abbasi, C. Abbey, C. Andrieu, U. Annakkage, S. Barsali, R. C. Campbell, R. Fletcher, F. Gao, T. Gaunt, A. Gole, N. Hatziargyriou, R. Irvani, G. Joos, H. Konishi, M. Kuschke, E. Lakervi, C.-C. Liu, J. Mahseredjian, F. Mosallat, D. Muthumuni, A. Orth, S. Papathanassiou, K. Rudion, Z. Styczynski, and S. C. Verma, "Benchmark Systems for Network Integration of Renewable and Distributed Energy Resources," CIGRE, Tech. Rep., 2014.
- [12] X. Wang, Y. W. Li, F. Blaabjerg, and P. C. Loh, "Virtual-impedance-based control for voltage-source and current-source converters," *IEEE Trans. on Power Electronics*, vol. 30, no. 12, pp. 7019–7037, 2015.
- [13] N. Omar, M. A. Monem, Y. Firooz, J. Salminen, J. Smekens, O. Hegazy, H. Gailous, G. Mulder, P. Van den Bossche, T. Coosemans, and J. Van Mierlo, "Lithium iron phosphate based battery – assessment of the aging parameters and development of cycle life model," *Applied Energy*, vol. 113, pp. 1575–1585, 2014.
- [14] X. Lu, K. Sun, J. M. Guerrero, J. C. Vasquez, and L. Huang, "State-of-charge balance using adaptive droop control for distributed energy storage systems in dc microgrid applications," *IEEE Transactions on Industrial Electronics*, vol. 61, no. 6, pp. 2804–2815, June 2014.
- [15] —, "Double-quadrant state-of-charge-based droop control method for distributed energy storage systems in autonomous dc microgrids," *IEEE Transactions on Smart Grid*, vol. 6, no. 1, pp. 147–157, Jan 2015.
- [16] R. Wang, Q. Sun, W. Hu, Y. Li, D. Ma, and P. Wang, "Soc-based droop coefficients stability region analysis of the battery for stand-alone supply systems with constant power loads," *IEEE Transactions on Power Electronics*, vol. 36, no. 7, pp. 7866–7879, 2021.
- [17] J. C. Vasquez, J. M. Guerrero, A. Luna, P. Rodriguez, and R. Teodorescu, "Adaptive droop control applied to voltage-source inverters operating in grid-connected and islanded modes," *IEEE Transactions on Industrial Electronics*, vol. 56, no. 10, pp. 4088–4096, 2009.
- [18] P. Kundur, N. Balu, and M. Lauby, *Power system stability and control*, ser. EPRI power system engineering series. McGraw-Hill, 1994.
- [19] D. P. Moran-Rio, J. Roldan-Perez, M. Prodanovic, and A. Garcia-Cerrada, "javier-roldan-perez/seamlesscoordinationmg: v01," May 2023. [Online]. Available: <https://doi.org/10.5281/zenodo.7924080>